International Journal of Refractory Metals & Hard Materials 88 (2020) 105178

Contents lists available at ScienceDirect

International Journal of Refractory Metals & Hard Materials

journal homepage: www.elsevier.com/locate/IJRMHM

Study of the welding procedure in nanostructured super-hard Fe- (Cr, Mo, W) - (C, B) hardfacing

Gramajo J.[a], A. Gualco[a,b,*], H. Svoboda[b,c]

[a] i4-CIC-Faculty of Engineering, National University of Lomas de Zamora, Argentina
[b] National Council Scientific Technical Research, CONICET, Argentina, CABA, Argentina
[c] GTSyCM3, INTECIN, School of Engineering, University of Buenos Aires (UBA), Av. Las Heras 2214 (1427), CABA, Argentina

ARTICLE INFO

Keywords:
Welding
Hardness
Microstructure
Carboborides

ABSTRACT

The optimization of the tribological properties of the surfaces by means of hardfacing techniques has made great progress in the metallurgical field in recent times. Alloys of the Fe-Cr-C and Fe-C-B type present excellent wear performance under severe conditions, where the incorporation of Nb, Mo and W improves the performance of severe abrasive wear. In this context, new semi-automatic welding consumables have been designed that deposit iron base material of high alloy, with complex carboborides of W, Mo and Cr which present very high hardness and resistant to abrasive wear. The purpose of this work was to compare microstructural variations coupons welded with one or two layers, with or without shielding gas. The chemical composition was measured on each coupon, the microstructure was characterized by X-ray diffraction and scanning electron microscopy. Dilution percentage was determined and Vickers microhardness profiles (HV2) were made on the different phases ($HV_{0.025}$). It was found that the dilution with and without shielding gas were 26% and 19%. The hardness was 960 and 1100 HV2. An increase in hardness was observed in the recrystallized areas, as well as a higher percentage of carboborides in the last bead.

1. Introduction

The improvement of the wear resistance of machine components can be achieved with proper deposition of hard layers of abrasion resistant materials [1]. The addition of alloy elements and rapid solidification generate fine microstructures that homogeneously distribute the hard phases producing an excellent combination of hardness and toughness [2]. The hard and thick phases of high hardness are important to achieve high abrasion resistance. The hardness of the hard phases and/or the hardness of the matrix must be greater than the hardness of the abrasive element [2,3].

Iron based alloys containing niobium (Nb), chromium (Cr) and molybdenum (Mo) in combination with boron (B) and carbon have been designed for hardfacing applications due to their high hardness and wear resistance [4]. Iron alloys with high chromium are widely used for the hardfacing of industrial components of mining, cement, thermal power plants and iron and steel industries, due to their high hardness and excellent abrasion resistance, which is attributed to the formation of chromium carbides [5,6]. The wear properties are affected by microstructures and by the amount of carbide phases. The thicker microstructures and with a small amount of carbides present a great loss of weight during abrasion [7]. In this regard, Fe-Cr-Nb-C-B consumables were manufactured to improve wear resistance performance with the addition of W and Mo that produce block-type carbides that improve the wear resistance and fracture of lengthened eutectic phases or carboborides. However, the control of carbide sizes and their distribution has become an important challenge for recharge alloys under study due to the fragility of primary lengthened carbides. Therefore, the wear resistance of hardfacing depends on many factors such as the type, shape and distribution of hard phases, as well as the toughness and behavior of the matrix [8]. In the semi-automatic welding process, all these factors aforementioned are strongly influenced by the welding procedure. The purpose of the following work is to study the influence of the number of layers and the shielding gas on the microstructure and microhardness of Fe-base- (Cr, Mo, W) - (C, B) alloy.

2. Materials and methods

The consumable used was a 1.6 mm diameter tubular wire, deposited by means of the semi-automatic welding process under gaseous protection and without it, with a free wire length of 20 mm.

Four coupons with 1 and 2 layers were welded, with Ar-20% CO2

* Corresponding author at: i4-CIC-Faculty of Engineering, National University of Lomas de Zamora, Argentina.
E-mail address: agustingualco@yahoo.com.ar (A. Gualco).

https://doi.org/10.1016/j.ijrmhm.2020.105178
Received 17 October 2019; Received in revised form 24 December 2019; Accepted 1 January 2020
Available online 02 January 2020
0263-4368/

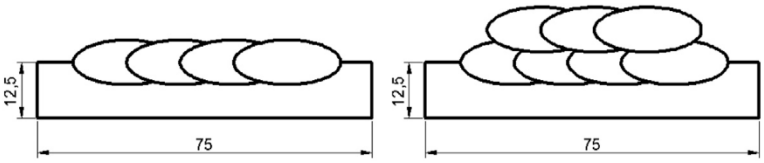

Fig. 1. Scheme of coupons; units in mm.

Table 1
Welding parameters.

Identification	Layers	Gases	Voltage [V]	Electrical power [A]	Welding speed [mm/s]	Heat Imput [kJ/mm]
A1	1	Ar-20 CO_2	35	300	3	3,5
A2	2	Ar-20 CO_2	35	300	3	3,5
O1	1	–	35	300	3	3,5
O2	2	–	35	300	3	3,5

and without gaseous protection. The parameters were chosen based on previous work [9,10]. The welding sequence was 4 beads for the first layer and 3 beads for the second layer, as shown schematically in Fig. 1. The stick out was 18 mm with gas, and 25 mm for the weld coupons without shielding gas. The welding parameters employed can be seen in Table 1. The welding position was flat; preheating and interpass temperatures were 150 °C.

The chemical composition was determined by optical emission spectrometry (OES). Boron was measured by plasma emission spectroscopy technique. Chemical composition measurements were made with energy dispersive X-ray spectrometry (EDS). The microstructure was characterized by scanning electronics (SEM). The dilution was calculated from the geometry of the beads using an image analysis software.

X-ray diffraction (XRD) was performed on the surface of the coupons. The equipment used was a RIGAKU, with radiation from Cu K-α. The scans were made from 35° to 95° with a speed of 1° per minute. The present phases were identified using a software for phase analysis. The crystallite size was determined using the Scherrer formula [11].

Transverse cuts were extracted from each of the welded coupons. Vickers micro-indentation profiles (HV2) were made horizontally, at 1 mm from the surface. The microhardness of the phases was calculated as the average of three measurements made with $HV_{0,025}$. Macro-indentation fracture toughness method was performed with Vickers macrohardness according to the ISO [12,13] and imposing a load from 294 to 2450 N at 10 s.

The abrasive wear tests were performed according to ASTM G65–15 method A, using the dry sand/rubber wheel apparatus. The 25 mm wide and 75 mm in length abrasion test coupons were cut from single- and double-layers deposits.

3. Results and discussion

3.1. Visual inspection

In Fig. 2 show the top view of the coupons.

It was observed that the A1 and A2 samples showed higher levels of spatters and little slag. This could be associated with the change of transfer mode the spray to globular repelled [14]. Most of the beads contained cracks, produced by the stress relief, which is normal for this type of deposits. The samples welded with two layers presented the higher number of cracks.

3.2. Macrography

Fig. 3 show cross section of the welded specimen where the base metal, weld deposit (hardfacing) and absence of macroscopic defects (pores, slag inclusions, cracks, etc.) can be observed.

The dilution of each sample was calculated using image analysis software. The A1 welded sample presented a dilution of 26% and the O1 of 19%. This would be related to the lower penetration, as a consequence of the change in the mode of transfer, and the greater volume of bead due to the increase in the stick out, from 18 to 25 mm, both factors produced a lower dilution. In addition, it was observed that the width of the beads increased with the welded samples without shielding gas. This would be related to the higher melting rate.

3.3. Chemical composition

Table 2 shows the result of the chemical analysis measured on the surface of the last bead.

The deposited material had a high concentration of alloy elements, within the Fe- (Nb, Cr, Mo, W) - (C, B) system. The obtained chemical composition tends to form amorphous structures, but because the cooling rate of the welded bead was less than the critical crystallization rate, ordered phases occurred as reported by different authors [15–18].

Table 2 shows a greater amount of alloy element in welded samples with two layers. This would be related to the level of dilution with the base metal. Furthermore, in the samples with the same number of layers it is observed that the difference was smaller due to slight dilution difference (from 19 to 25%) and to the transfer of alloy elements to the slag in the welded without shielding gas.

3.4. Microstructural characterization

Fig. 4 shows the DRX patterns obtained for all conditions.

In Fig. 4 it can be seen that the microstructure was formed by α-Fe and γ-Fe, detecting the presence of carboborides ((Cr,Fe)7(B,C)3, (Cr,Fe)23(B,C)6) [18,19]. Nb carbides were also identified in all samples. The crystal size in α-Fe was between 50 and 150 nm. The percentage of carbides and carboborides were greater with two layers. A slight increase in γ-Fe and carboborides (Cr,Fe)7(B,C)3 was observed in the welded samples under shielding gas and with two layers. This would be associated with the higher cooling rate and the higher content of alloying elements.

Fig. 5 show two Backscattered-Electron images (BSE) from the A2 and O2 sample. A large dispersion of hard precipitates can be distinguished in block and needles shapes homogeneously distributed. The percentage of them was around 65%, which is consistent with what was observed in the diffraction patterns.

It can be seen niobium carbides of 2 to 4 μm size, Mo/W carboborides with form of a block of 10-25 μm in the first layer and 17–41 μm for the two-layer, the eutectic formed of flat and globular precipitates of the $M_{23}X_6$ type of thickness 1 to 3 μm in a α-Fe matrix and elongated carbides M_7X_3 of 10 to 15 of wide being thicker in O2 sample. As reported in the literature [18], the NbC were the first carbides to appear during the solidification process. Subsequently, with the decrease of the temperature, growing clusters of Mo/W carboborides. This was confirmed by maps of chemical compositions in Fig. 6. Finally,

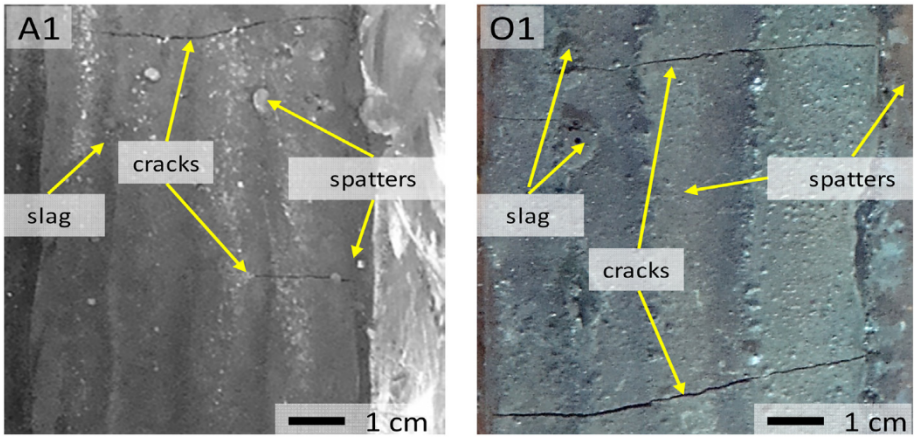

Fig. 2. Top view of welded coupons A1 and O1.

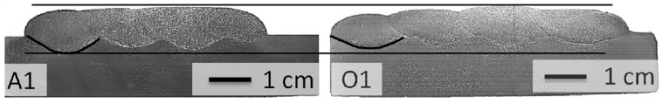

Fig. 3. Macrograph of cross sections of coupons.

Table 2
Chemical composition of all weld metal (% by weight).

	C	Mn	Cr	Nb	Mo	W	B
A1	1.49	0.39	14.3	5.5	3.2	5.7	4.8
O1	1.60	0.39	14.9	5.7	3.4	6.1	4.9
A2	1.60	0.34	17.1	7.2	4.0	7.5	5.1
O2	1.70	0.37	18.1	7.3	4.1	7.8	5.1

the eutectic, α o γ-Fe and M7X3 M_7X_3, was formed from the remaining liquid.

The dark primary carboborides, dark eutectic carboborides, and bright eutectic carboborides were found in the microstructure, Fig. 6a and b. Considering the stoichiometric ratio of the elements in the microstructure, primary dark carboborides of the M7(CB)3, eutectic dark carboborides of the M7(CB)3 and eutectic bright carboborides of the M23(CB)6 are scattered in the ferritic matrix.

3.5. Microhardness

Fig. 7 shows the microhardness of phases. These values are the average of 3 measurements made on each phase with $HV_{0,025}$.

It can be seen in Fig. 7 that the phase microhardness was: 1460 HV for niobium carbides, 1150 HV for Mo/W carbides, 920 HV for Fe/Cr carbides and 695 HV for the eutectic. The microhardness of the eutectic zone varied depending on the number of layers being lower for the welded samples with protection gas. This would be related to the decrease in the amount by volume of the $M_{23}X_6$ eutectic carbide.

Fig. 8 shows the horizontal hardness profiles of the different coupons.

Fig. 8 shows the hardness HV2 of the deposit which were between 900 and 1100 HV. This is consistent with reported for this type of materials [18,19]. It can be seen that the samples with two layers had the greatest hardness. This would be explained by a high fraction of hard phases in both conditions due to its higher content of alloy elements, see Table 2. No large differences were observed depending on the type of shielding protection.

3.6. Features toughness

In Fig. 9 shows the relationship between crack and load applied for all conditions.

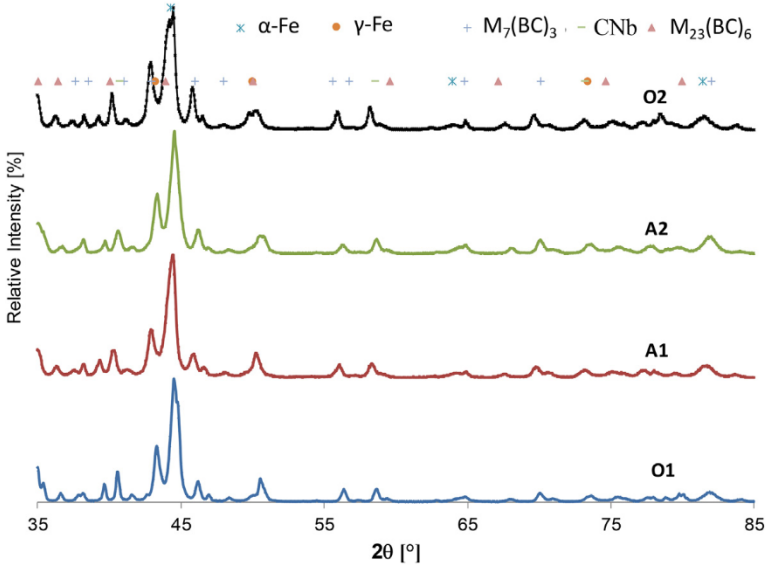

Fig. 4. DRX patterns of all conditions.

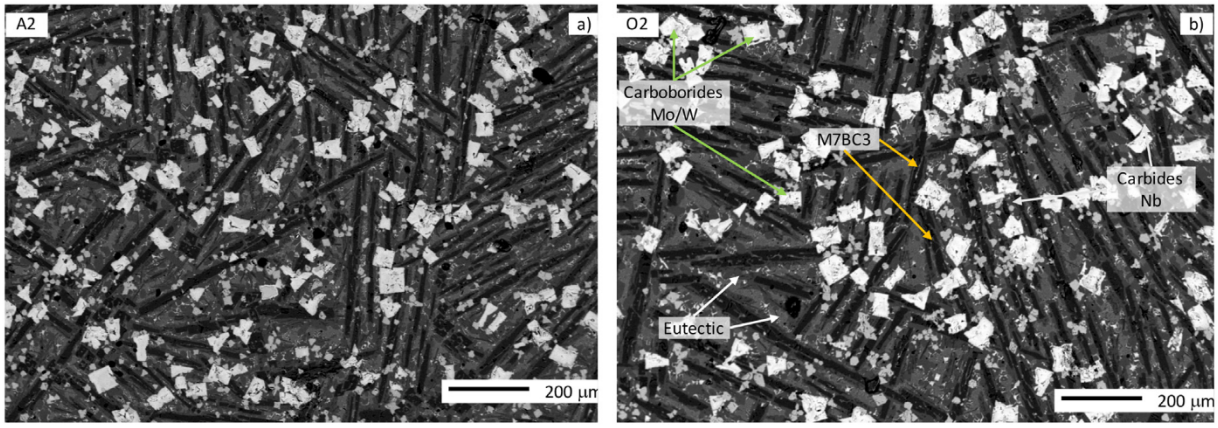

Fig. 5. Microstructures of samples a) A2 and b) O2.

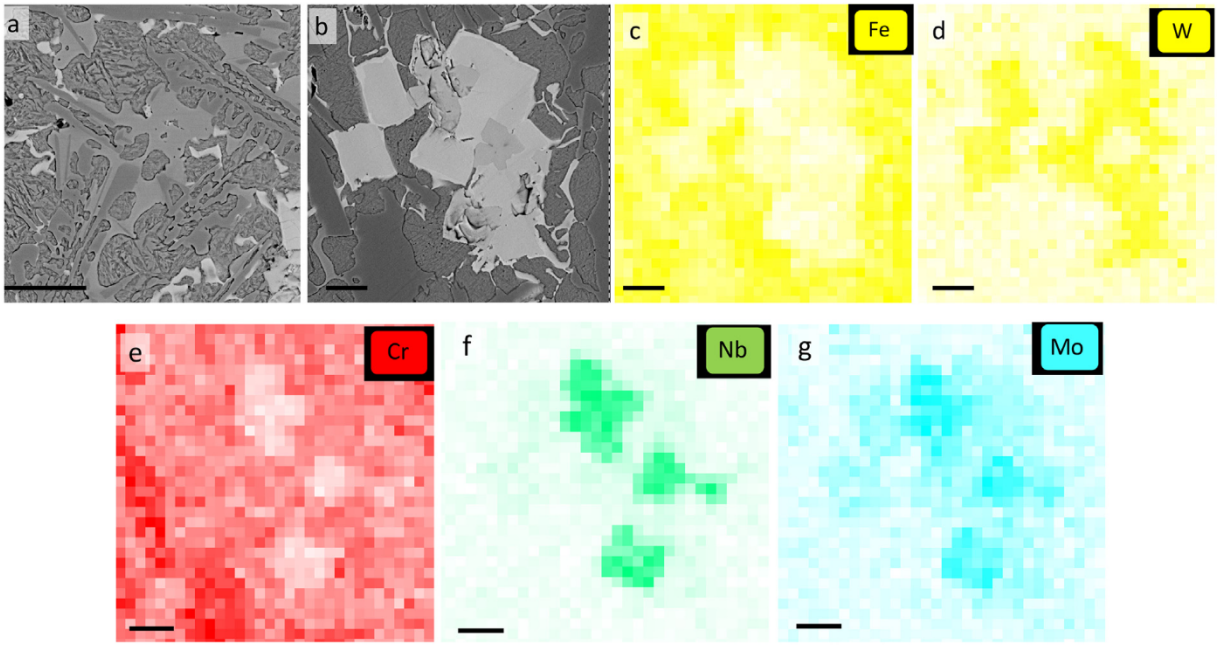

Fig. 6. a) Backscattered-Electron (BSE) of core-shell carbodorides $M_{23}X_6/M_7X_3$, b) O1 and c) A2. b) BSD of NbC cluster and complex carboborides with chemical compositions maps of c) Fe d) W, e) Cr, f) Nb and g) Mo.

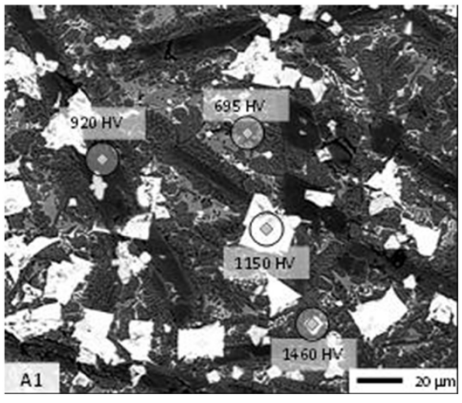

Fig. 7. Phase microhardness measurements performed on coupon A1.

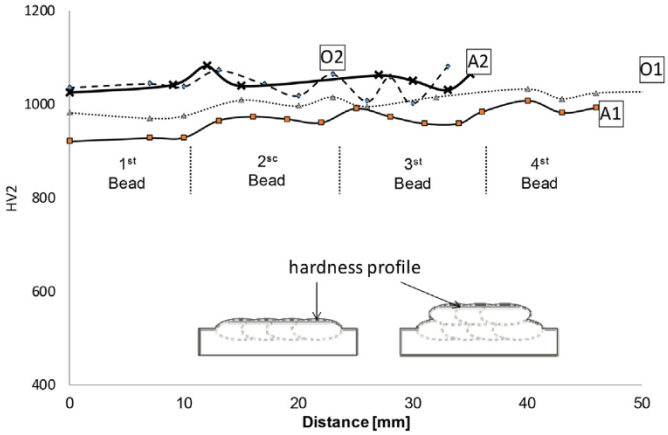

Fig. 8. Hardness of the coupons at 1 mm from the top surface.

The fracture toughness was computed using Shetty's equation [20]. The coefficient of Poisson (ν) for iron was considered 0.29, half of the indenter tip angle (ψ), which is 68°; H is hardness (in MPa); P is force and 4a is total linear crack length [20]. It can be seen that during transgranular fracture in primary M7C3 easier growth of cracks were in the longitudinal direction of columnar M7C3 [21,22]. Fracture toughness were 28.7 MPa√m and 28.8 MPa√m for A1 and O1 and

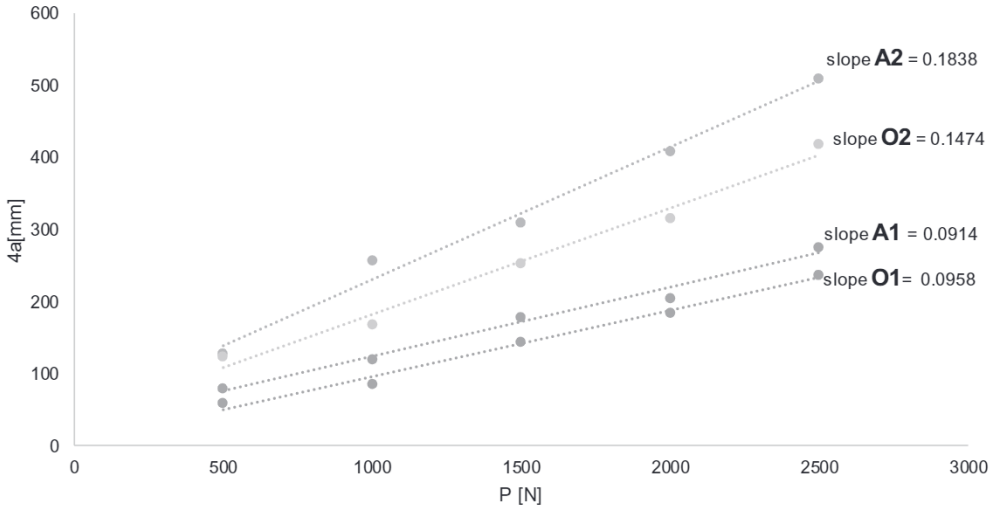

Fig. 9. Crack length variation caused by changing the applied force to the Vickers indenter.

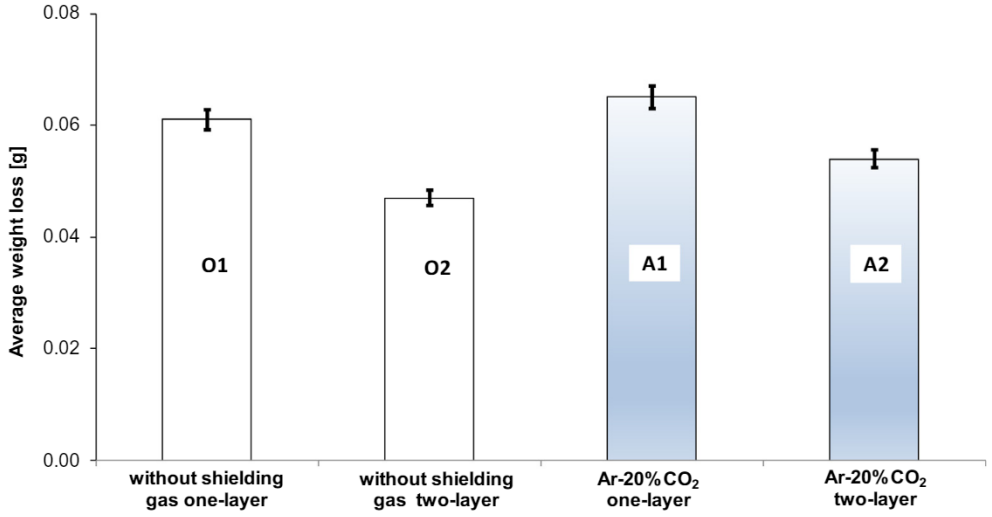

Fig. 10. Wear for all samples.

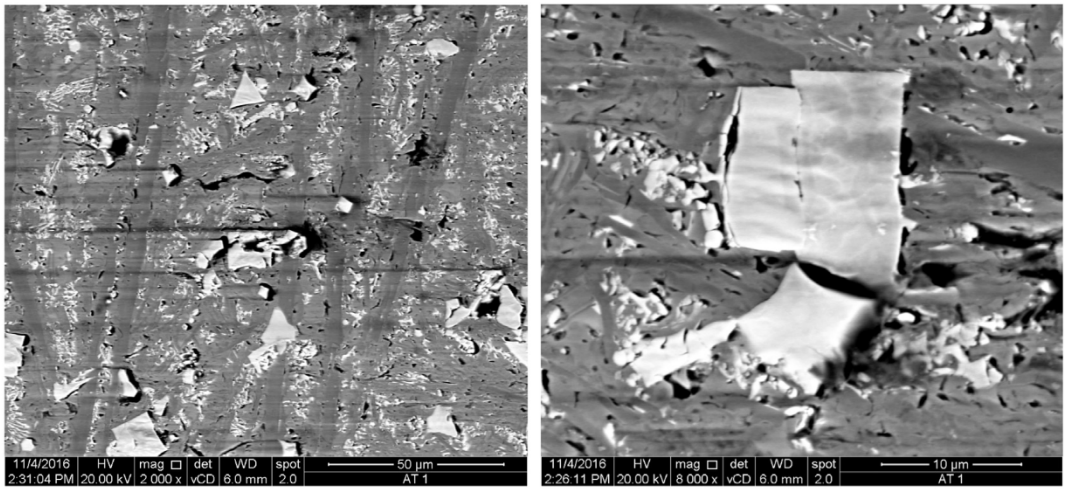

Fig. 11. Worn surface for A1 samples.

21.8 MPa√m and 25.0 MPa√m for A2 and O2 respectively. These differences would be associated with the quantity and size of M7 BC3 which were thicker and more elongated in O2 sample, see Fig. 5.

3.7. Abrasive wear

The results of wear test are presented in the Fig. 10. The two-layer samples showed a 20 to 30% higher wear resistance, relative to those of only one layer, result associated to the higher degree of alloying elements. Samples welded without gas shielding had higher wear resistance.

The worn mechanisms were fragmentation, pulling out, and ploughing (Fig. 11). The best abrasion resistance was obtained in the second layer of the complex carbides deposit, in which the elevated volume fraction of M7X3 carboborides provided a barrier against indentation, grooving and cutting [23,24]. This beneficial effect is probably reinforced by cluster of NbC and M23X6 complex carboborides [25,26].

4. Conclusions

- The deposited material presented a high concentration of alloy elements, within the Fe- (Nb, Cr, Mo, W) - (C, B) system.
- The microstructure was formed by α-Fe and γ-Fe, detecting the presence of metal carboborides ($(Cr,Fe)_7$ $(B,C)_3$, $(Cr,Fe)_{23}$ $(B,C)_6$). Nb carbides were also identified for all samples. The percentage of carbides and carboborides was greater than 65%. A slight increase in γ-Fe and carboborides $(Cr, Fe)_7(B, C)_3$ was observed in the welded samples under gas protection and with two layers.
- The hardness of the deposit was between 900 and 1100 HV. The samples with two layers presented the greatest hardness. No major differences were observed depending on the type of shielding protection.
- Samples welded with two layer presented better wear resistance and minor toughness associated mainly with higher presence of M7X3.

Declaration of Competing Interest

The authors declare that they have no known competing financial interests or personal relationships that could have appeared to influence the work reported in this paper.

Acknowledgement

The authors are grateful to EUTECTIC-CONARCO Argentina, to AIR LIQUIDE Argentina, to EUTECTIC-USA, to the INTI - MECHANICAL ELECTRONIC MICROSCOPY LABORATORY for the realization of scanning electron microscopy and APUEMFI for financial support for this project.

References

[1] J.M. Amado, M.J. Tobar, J.C. Alvarez, J. Lamas, A. Yáñez, Laser cladding of tungsten carbides (Spherotene1) hardfacing alloys for the mining and mineral industry, Appl. Surf. Sci. 255 (2009) 5553–5556.
[2] E. Badisch, C. Katsich, H. Winkelmann, F. Franek, M. Roy, Wear behaviour of hardfaced Fe–Cr–C alloy and austenitic steel under 2-body and 3-body conditions at elevated temperature, Tribol. Int. 43 (2010) 1234–1244.
[3] J.J. Coronado, H.F. Caicedo, A.L. Gómez, The effects of welding processes on abrasive wear resistance for hardfacing deposits, Tribol. Int. 42 (2009) 745–749.
[4] G. Azimi, M. Shamanian, Effect of silicon content on the microstructure and properties of Fe–Cr–C hardfacing alloys, J. Mater. Sci. 45 (2010) 842–849.
[5] S.G. Sapate, A. Selokar, N. Garg, Experimental investigation of hard faced martensitic steel under slurry abrasion conditions, Mater Des. 31 (8) (2010) 4001–4006.
[6] J.H. Kim, K.H. Ko, S.D. Noh, G.G. Kim, S.J. Kim, The effect of boron on the abrasive wear behavior of austenitic Fe-based hardfacing alloys, Wear 267 (2009) 1415–1419.
[7] Q.Y. Hou, Y.Z. He, Q.A. Zhang, J.S. Gao, Influence of molybdenum on the microstructure and wear resistance of nickel-based alloy coating obtained by plasma transferred arc process, Mater Des. 28 (6) (2007) 1982–1987.
[8] M.F. Buchely, J.C. Gutierrez, L.M. León, A. Toro, The effect of microstructure on abrasive wear of hardfacing alloys, Wear 259 (2005) 52–61.
[9] N.J. Gramajo, A. Gualco, H.G. Svoboda, E.S. Surian, Influence of Heat Input in (Cr, Mo, W, Nb, C, B) Fe-Based Nanostructured Hardfacing Deposited by FCAW, XLI Consolda, Salvado Bahia, Brasil, 12–15, Octubre (2015).
[10] N.J. Gramajo, A. Gualco, H.G. Svoboda, E.S. Surian, Caracterización microestructural de depósitos nanoestructurados base Fe-(Nb,Cr,Mo,W)-(C,B). SAM/CONAMET, 17–20 de noviembre (2015) (Concepción, Chile).
[11] B.D. Cullity, S.R. Stock, Elements of X-ray diffraction, 3 ed., Prentice Hall, 2001 (520 p).
[12] ISO 28079, Hardmetals - Palmqvist Toughness Test, International Organization for Standardization, Geneva (Switzerland, 2009.
[13] ISO 6507–1, Metallic Materials - Vickers Hardness Test - Part 1: Test Method, International Organization for Standardization, Geneva (Switzerland, 2005.
[14] J. Norrish, Advanced Welding Process-Technologies and Process Control, Woodhead Publishing Limited, 2006.
[15] A. Inoe, Amorphous and Nanocrystalline Materials: Preparation, Properties, and Applications, Springer, 2010, p. 206.
[16] H. Gleiter, Nanostructured materials: basic concepts and microstructure, Acta Mater. 48 (1) (2000) 1–29.
[17] J. Weissmiiller, Some basic notions on nanostructured solids, Mater. Sci. Eng. A 179–180 (1994) 102–107.
[18] D.J. Branagan, M.C. Marshall, B.E. Meacham, High toughness high hardness iron based PTAW weld materials, Mater. Sci. Eng. A 428 (2006) 116–123.
[19] M. Kirchgabner, E. Badish, F. Franek, Behaviour of iron-based hardfacing alloys under abrasión and impact, Wear 265 (2008) 772–779.
[20] D.K. Shetty, I.G. Wright, P.N. Mincer, A.H. Clauer, Indentation fracture of WC-co cermets, J. Mater. Sci. 20 (1985) 1873–1882.
[21] J.J. Coronado, Effect of (Fe,Cr)7C3 carbide orientation on abrasion wear resistance and fracture toughness, Wear 270 (2011) 287–293.
[22] Mohtasham Bahoosh, Hamid Reza Shahverdi, Amirreza Farnia, Macro-indentation fracture mechanisms in a super-hard hardfacing Fe-based electrode, Eng. Fail. Anal. 92 (October 2018) 480–494.
[23] K.H. Zum Gah, Wear by hard particles, Tribol. Int. 31 (10) (1998) 587–596.
[24] H. Fujimura, A. Notomi, Development of Hard Overlay Welding for High Wear Resistance; IIW DOC XII-1071-88, (1988).
[25] E.O. Correa, N.G. Alcântara, D.G. Tecco, R.V. Kumar, The relationship between the microstructure and abrasive resistance of a hardfacing alloy in the Fe-Cr-C-Nb-V system, Metall. Mater. Trans. A 38 (8) (2007) 1671–1680.
[26] S. Pawar, A.K. Jha, G. Mukhopadhyay, Effect of different carbides on the wear resistance of Fe-based hardfacing alloys, Int. J. Refract. Met. Hard Mater. 78 (January 2019) 288–295.